Theoretical investigation of the pressure broadening D_1 and D_2 lines of cesium atoms colliding with ground-state helium atoms

Moussaoui Abdelaziz[1], Alioua Kamel[1,2,†], Allouche Abdul-rahman[3], and Bouledroua Moncef[4]

[1] *Université Chérif Messaidia, B. P.* 1553, *Souk-Ahras* 41000, *Algerie*

[2] *Laboratoire de Physique de la Matière et du Rayonnement LPMR, Université Chérif Messaidia, B. P.* 1553, *Souk-Ahras* 41000, *Algerie*

[3] *Université Lyon* 1, *CNRS, LASIM UMR*5579, *bât. A. Kastler,* 43 *Bd du* 11 *novembre* 1918, *F*-69622 *Villeurbanne, France*

[4] *Laboratoire de Physique des Rayonnements LPR, Université Badji Mokhtar, B. P.* 12, *Annaba* 23000, *Algerie*

(Received 18 June 2019; revised manuscript received 23 August 2019; published online 24 September 2019)

Full quantum mechanical calculations are performed to determine the broadening in the far wings of the cesium D_1 and D_2 line shapes arising from elastic collisions of Cs atom with inert helium atoms. The potential energy curves of the low-lying CsHe molecular states, as well as the related transition dipole moments, are carefully computed from *ab initio* methods based on state-averaged complete active space self-consistent field–multireference configuration interaction (SA-CASSCF–MRCI) calculations, involving the spin–orbit effect, and taking into account the Davidson and BSSE corrections. The absorption and emission reduced coefficients are determined in the temperature and wavelength ranges of 323–3000 K and 800–1000 nm, respectively. Both profiles of the absorption and the emission are dominated by the free–free transitions, and exhibit a satellite peak in the blue wing near the wavelength 825 nm, attributed to $B^2\Sigma^+_{1/2} \longrightarrow X^2\Sigma^+_{1/2}$ transitions. The results are in good agreement with previous experimental and theoretical works.

Keywords: absorption coefficient, emission coefficient, pressure broadening, potential curves

PACS: 32.80.–t, 31.50.Bc, 31.50.Df, 32.70.Jz **DOI:** 10.1088/1674-1056/ab4043

1. Introduction

The principal and dominant alkali-metal D_1 and D_2 lines, broadened by elastic collisions with rare-gases, have been a subject of many theoretical and experimental studies. More precisely, the determination of the profiles and satellite features in the wings of the heavy alkaline atoms evolving in the bath of He atoms has been, very recently, the goal of several theoretical[1–7] and experimental[5,8,9] works.

On the other hand, the spectroscopic studies of the alkali–rare-gas system have demonstrated their significance in a few fields, such as astrophysics and laser physics. In fact, the experimental measurement or theoretically simulation of the absorption–emission spectra must be a crucial tool for determining the physical and chemical properties of the environments of extrasolar giant planets and brown dwarfs.[10–16] Furthermore, the analysis of the collisionally induced spectral broadening of the D_1 and D_2 lines has played a very significant role in the conceptual design and manufacturing of several new type and efficient lasers, namely, the diode-pumped alkali lasers (DPAL),[7,17–20] and the excimer-pumped alkali vapor lasers (XPAL),[21–24] which was proposed as an alternative to high-power diode-pumped solid-state lasers, and could be used not only for technological applications but also for very important medical application in magnetic resonance imaging.

As far as we know, the photoabsorption profiles generated by the pressure-broadening of D_1 and D_2 lines of cesium atom immersed in a bath of diluted helium gas has been studied theoretically, in the frame work of classical theory, by Allard *et al.*[1] and Hager *et al.*[5] using the unified and Anderson–Tallman theories, respectively. In addition, the photoemission profiles are experimentally realized by Hedges *et al.*,[8] however, the photoabsorption spectra are very recently measured by Hager *et al.*[5]

The primary focus of the current work is to determine, in the framework of purely quantum mechanical study, the photoabsorption and photoemission profiles of the D_1 and D_2 lines of the cesium atom perturbed by the helium one, and the satellite features appearing in the wings. We also analyze carefully the behavior of the shape profiles, the form of the satellites, and their positions at certain well-defined temperature values.

For this purpose, we start with calculating the potential-energy curves (PECs) of the low-lying CsHe molecular states, namely, the ground $X^2\Sigma^+_{1/2}$ and the excited $A^2\Pi_{1/2}$, $A^2\Pi_{3/2}$, and $B^2\Sigma^+_{1/2}$ states, and the transition dipole moments (TDMs) for the allowed transitions, that is to say, $D_{\Sigma_{1/2}-\Pi_{1/2}}$, $D_{\Sigma_{1/2}-\Pi_{3/2}}$, and $D_{\Sigma_{1/2}-\Sigma_{1/2}}$. The *ab initio* calculations are performed at different levels of theory, starting with the state-averaged complete active space self-consistent field (SA-CASSCF) followed by the multireference configuration interaction (MRCI) method with Davidson correction, and ending by the spin–orbit (SO) coupling effects including the basis-set superposition error (BSSE) corrections. All these methods are implemented in MOLPRO package.[25] In order to assess the accuracy of the obtained PECs and TDMs curves,

†Corresponding author. E-mail: kamel.alioua@univ-soukahras.dz

we have determined their spectroscopic parameters, and the ro-vibrational energy levels of the molecular states. To ensure the quality of the absorption–emission profiles and satellite features, the results are finally compared with previous theoretical and available experimental work.

2. Pressure broadening coefficients

We are interested, in this work, in the far-wing profiles arising from $D_1\left(6^2S_{1/2}-6^2P_{1/2}\right)$ and $D_2\left(6^2S_{1/2}-6^2P_{3/2}\right)$ resonance lines of Cs atoms in the presence of the ground helium He($1s^2$) atoms. We assume that the density of the Cs–He gas mixture under thermal equilibrium is sufficiently low to consider only the binary collisions between these two types of atoms. Therefore, the problem of pressure broadening can be easily reduced to temporarily formed CsHe quasi-molecule.

We must precise that during the transition process, the first broadened D_1 line of absorber–perturber is attributed to the transitions between the ground $X^2\Sigma^+_{1/2}$ state and the first excited $A^2\Pi_{1/2}$ state of CsHe quasi-molecule, while the second broadened D_2 line is attributed to the contribution of transitions between the ground $X^2\Sigma^+_{1/2}$ state and the second excited $A^2\Pi_{3/2}$ state on one hand, and between the $X^2\Sigma^+_{1/2}$ state and the third excited $B^2\Sigma^+_{1/2}$ state on the other hand. Since both $X^2\Sigma^+_{1/2}$ and $B^2\Sigma^+_{1/2}$ states are dominantly repulsive whereas the $A^2\Pi_{1/2}$ and $A^2\Pi_{3/2}$ states are less deep, we consider in such case only the free–free (ff) and free–bound (fb) transitions.

In the following, we will especially focus on the determination of reduced coefficients of the photoabsorption and the photoemission.

2.1. Absorption coefficients

One can characterize the pressure-broadened profile of the cesium D_1 or D_2 resonance line in the presence of the helium He($1s^2$) atoms by defining the temperature-dependent reduced absorption coefficient $\alpha_r(\nu)$ at frequency ν in such way that the free–free reduced absorption coefficients $\alpha_r^{ff}(\nu)$, at frequency ν,[26,27] corresponding to transitions from the lower (l) to upper (u) continuum levels, are expressed at temperature T by

$$\alpha_r^{ff}(\nu) = \frac{8\pi^3\nu}{3c}\omega\left(\frac{h^2}{2\pi\mu k_B T}\right)^{3/2}\int_0^\infty d\varepsilon_u\sum_J(2J+1) \times\left|\left\langle g_u^{\varepsilon_u J}\left|D(R)\right|g_l^{\varepsilon_l J}\right\rangle\right|^2\exp\left(-\frac{\varepsilon_l}{k_B T}\right), \quad (1)$$

where the symbols appearing in this formula, namely, c, h, k_B, and stand for the speed of light, the Plank's constant, the Boltzmann's constant, and the reduced mass, respectively. The electronic energy levels, ε_l and ε_u, are related via the relationship

$$\varepsilon_l = h(\nu_0-\nu)+\varepsilon_u, \quad (2)$$

with ν_0 being the frequency of the D_1 or D_2 resonance line. Moreover, the free–bound reduced absorption coefficients $\alpha_r^{fb}(\nu)$ derived for the transitions from all lower continuum levels to a set of upper bound levels are given by the relation

$$\alpha_r^{fb}(\nu) = \frac{8\pi^3\nu}{3c}\omega\left(\frac{h^2}{2\pi\mu k_B T}\right)^{3/2}\sum_{vJ}(2J+1) \times\left|\left\langle g_u^{vJ}\left|D(R)\right|g_l^{\varepsilon_l J}\right\rangle\right|^2\exp\left(-\frac{\varepsilon_l}{k_B T}\right), \quad (3)$$

where the integer numbers J and v are the rotational and vibrational quantum numbers, respectively. The factor ω is the probability that a transition takes place towards a final state. The transition factors corresponding to the $A^2\Pi_{1/2}$, $A^2\Pi_{3/2}$, and $B^2\Sigma^+_{1/2}$ states are $\omega=1$, $\omega=2/3$, and $\omega=1/3$, respectively.

We notice that the rotational quantum numbers J involved in the computations are generally very large. It is, therefore, possible to assume $J_u \simeq J_l = J$. The transition dipole moment is defined by $D(R)=\left|\left\langle\chi_f(\boldsymbol{r},\boldsymbol{R})\right|e\sum\boldsymbol{r}_i\left|\chi_i(\boldsymbol{r},\boldsymbol{R})\right\rangle\right|$ where $\boldsymbol{r}_i$ is the coordinate of the i-th electron, $\boldsymbol{r}$ stands for all electronic coordinates, and $\chi(\boldsymbol{r},\boldsymbol{R})$ is the electronic wave function at the internuclear distance R.

Furthermore, the radial-wave functions $g(R)$, as well as the transition dipole moments $D(R)$, are needed to compute the matrix elements shown in Eqs. (1) and (5), which vary with the nuclear separation R, and the wave functions are the solutions of radial Schrödinger equation

$$\frac{d^2g(R)}{dR^2}+\frac{2\mu}{\hbar^2}\left[\varepsilon-V(R)-\frac{J(J+1)\hbar^2}{2\mu R^2}\right]g(R)=0, \quad (4)$$

where $V(R)$ is the electronic potential energy of the CsHe system at hand and ε is the energy of the relative motion. Note that the free wavefunctions $u(R)=u^{\varepsilon J}(R)$ are energy-normalized, while the bound wavefunctions $u(R)=u^{vJ}(R)$ are rather space-normalized, and both ε and $V(R)$ are measured with respect to the respective dissociation limits.

2.2. Emission coefficients

For the emission spectra, we consider for the D_1 line the bound–free and free–free transitions between the $A^2\Pi_{1/2}$ and $X^2\Sigma^+_{1/2}$ states. For the D_2 line, we take into consideration the two bound–free and free–free transitions between the $A^2\Pi_{3/2}$ and $X^2\Sigma^+_{1/2}$ states and only free–free transitions between the $B^2\Sigma^+_{1/2}$ and $X^2\Sigma^+_{1/2}$ states.

On one hand, the free–free reduced emission coefficients $k_r^{ff}(\nu)$ are given at temperature T by[28–30]

$$k_r^{ff}(\nu) = \frac{64\pi^4\nu^3}{3hc^3}\omega\left(\frac{h^2}{2\pi\mu k_B T}\right)^{3/2}\int_0^\infty d\varepsilon_u\sum_J(2J+1) \times\left|\left\langle g_u^{\varepsilon_u J}\left|D(R)\right|g_l^{\varepsilon_l J}\right\rangle\right|^2\exp\left(-\frac{\varepsilon_u}{k_B T}\right), \quad (5)$$

and on the other hand, the bound–free reduced emission coefficients $k_{\mathrm{r}}^{\mathrm{bf}}(\nu)$ are expressed by

$$k_{\mathrm{r}}^{\mathrm{bf}}(\nu) = \frac{64\pi^4\nu^3}{3hc^3}\omega\left(\frac{h^2}{2\pi\mu k_{\mathrm{B}}T}\right)^{3/2}\sum_{vJ}(2J+1) \times\left|\left\langle g_{\mathrm{u}}^{vJ}\left|D(R)\right|g_{\mathrm{l}}^{\varepsilon_{\mathrm{l}}J}\right\rangle\right|^2\exp\left(-\frac{\varepsilon_{\mathrm{u}}}{k_{\mathrm{B}}T}\right). \quad (6)$$

In the equations cited above (Eqs. (1), (3), (5), and (6)), it appears clearly that for every internuclear distance R, the electronic interaction potentials $V(R)$ of molecular states and the corresponding transition dipole moments $D(R)$ must be determined accurately.

3. Potential energy curves and transition dipole moments

We investigate the fourth low-lying doublet electronic states of the molecule CsHe using complete active space self consistent field (CASSCF) procedure followed by a multireference configuration interaction with Davidson correction treatment for the electron correlation. The energies for Ω states have been obtained using the state-interacting method, which means that the spin–orbit eigenstates are obtained by diagonalizing $\hat{H}_{\mathrm{el}}+\hat{H}_{\mathrm{SO}}$ in a basis of eigenfunctions of $\hat{H}_{\mathrm{el}}$, where $\hat{H}_{\mathrm{el}}$ is the electronic Hamiltonian and $\hat{H}_{\mathrm{SO}}$ is the spin–orbit pseudo-potential. $\hat{H}_{\mathrm{el}}$ elements matrix are calculated at CASSCF/MRCI level of method and the spin–orbit coupling terms are calculated using a spin–orbit pseudo potential. The basis set superposition error (BSSE) is taken into account using the counterpoise method (CP) approach.[31] All calculations are made using the computational chemistry program Molpro.[25]

We use the aug-cc-pCV5z[32] basis set for helium atom while the small Stugrart relativistic pseudopotential is used for Cs atom,[33] with its corresponding basis set for s, p, d, and f, and after small modifications for the last four exponents p basis set that become: $0.121000, 0.065500, 0.016200, 0.0061$ with two additional ones which are $0.0026, 0.0016$ and leaving intact their coefficients. The change are also made on the last two sets of three parameters that belong to the term series of p spin–orbit pseudopotential. These two sets of parameters are: $(2, 2.280961580, -23.7438456037161)$ and $(2, 2.103490505, 23.7485580204565)$.

In this pseudo potential, only 9 electrons are explicitly considered. In CsHe molecule, the s and p inner orbitals of Cs and the 1s of He are considered as closed orbitals and 1 valence electron is explicitly treated using 6 active orbitals in our CASSCF calculation. The correlations of inner electrons are treated at MRCI level of theory. All computations are performed without symmetry.

Table 1 shows our calculated energy transitions for $^2\mathrm{P}_{1/2}$ and $^2\mathrm{P}_{3/2}$ states for Cs atom. Compared to experimental values,[34,35] we are able to reproduce these values with an error of only 11 cm^{-1} corresponding to a relative error of about 0.09%. For CsHe molecule, the potential energy curves and the dipole moment functions are performed over the interval 2 Å $\leq R \leq$ 46 Å for the fourth states considered in our calculation, namely, $\mathrm{X}^2\Sigma^+_{1/2}$, $\mathrm{A}^2\Pi_{1/2}$, $\mathrm{A}^2\Pi_{3/2}$, and $\mathrm{B}^2\Sigma^+_{1/2}$. From now, in order to lighten the writing, we use, if necessary, the following non-conventional notation for the above-mentioned states, i.e., $\mathrm{X}_{1/2}$, $\mathrm{A}_{1/2}$, $\mathrm{A}_{3/2}$, and $\mathrm{B}_{1/2}$. The energy curves of the $\mathrm{X}_{1/2}$, $\mathrm{A}_{1/2}$, $\mathrm{A}_{3/2}$, and $\mathrm{B}_{1/2}$ states are shown in Fig. 1. Likewise, the transition dipole moments $D_{\Sigma_{1/2}-\Pi_{1/2}}$, $D_{\Sigma_{1/2}-\Pi_{3/2}}$, and $D_{\Sigma_{1/2}-\Sigma_{1/2}}$ of the $\mathrm{A}_{1/2} \leftarrow \mathrm{X}_{1/2}$, $\mathrm{A}_{3/2} \leftarrow \mathrm{X}_{1/2}$, and $\mathrm{B}_{1/2} \leftarrow \mathrm{X}_{1/2}$ transitions, respectively, are shown in Fig. 2. Their corresponding spectroscopic constants are given in Table 3. It is clear that both $\mathrm{X}_{1/2}$ and $\mathrm{B}_{1/2}$ states are mostly repulsive, whereas the $\mathrm{A}_{1/2}$ and $\mathrm{A}_{3/2}$ states have very shallow wells. Compared to available theoretical values in literature,

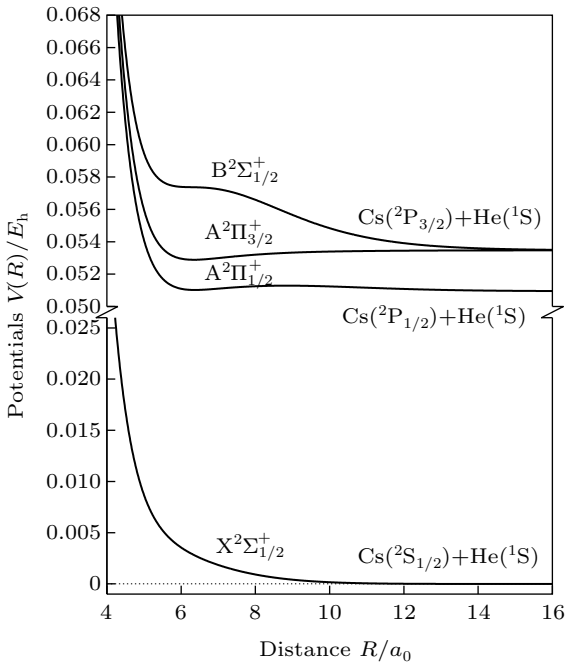

Fig. 1. CsHe potential-energy curves $V(R)$ (in a.u.) for the ground $\mathrm{X}^2\Sigma^+_{1/2}$ and excited $\mathrm{A}^2\Pi_{1/2}$, $\mathrm{A}^2\Pi_{3/2}$, and $\mathrm{B}^2\Sigma^+_{1/2}$ molecular states.

Table 1. Calculated atomic energy levels (in cm^{-1}) of the Cs atom compared with results from National Institute of Standards and Technology (NIST) recommended data.

	This work		NIST data
	Modified ECP	No modified ECP	
$^2\mathrm{P}_{1/2}$	11189.34181699	11284.67560750	$11178.26815870 \pm 0.00000008$[34]
$^2\mathrm{P}_{3/2}$	11743.3714317	11695.7044712	$11732.3071041 \pm 0.0000002$[35]

the equilibrium distances for the $X_{1/2}$ and $B_{1/2}$ states are close to each other, and the well depth of $X_{1/2}$ state is shallower than that calculated by Blank *et al.*[2] and comparable with these of Medvedev *et al.*[36] while our calculated value of dissociation energy of $B_{1/2}$ state is three times bigger than that calculated by Blank *et al.*[2] For $A_{1/2}$, our calculated equilibrium distance and dissociation energy are very close to those calculated by Blank *et al.*,[2] Zbiri *et al.*,[37] and Enomoto *et al.*[38] The potential of $A_{1/2}$ has a barrier and a second minimum at long distance. Our barrier measured from the dissociation limit is about 74.2 cm^{-1} at $R = 4.7$ Å, in very good agreement with 75.2 cm^{-1} at $R = 5.0$ Å obtained by Enomoto *et al.*[38] and in agreement with 57.7 cm^{-1} at $R = 4.87$ Å obtained by Blank *et al.*[2] Our second minimum has a well of -0.25 cm^{-1} from the dissociation limit, located at 10.6 Å to be compared to -1.9 cm^{-1} at $R = 9.2$ Å obtained by Blank and his coworkers. Concerning $A_{3/2}$, our calculated spectroscopic constants are close to that predicted by Blank *et al.* while there is a disagreement with values calculated by Pascal *et al.* and by Zbiri *et al.* The vibrational energy levels of $A_{1/2}$ and $A_{3/2}$ have been calculated by Blank *et al.* using an *ab initio* method and by Enomoto *et al.* using a semi-empirical approach to take account of the spin–orbit effect. These values and ours are shown in Table 2. For $A_{1/2}$, only one vibrational state is predicted in all works with a good agreement for energy level between our value and that predicted by Blank *et al.*[2] and by Enomoto *et al.*[38] However, for $A_{3/2}$, we have predicted four states while six vibrational states have been predicted by Blank *et al.*[2] and five ones by Enomoto *et al.*[38] Note that only three vibrational states have been observed experimentally.[38] To our knowledge, the experimental spectroscopic constants are not yet available in literature. The dipole moment functions from the three electronic excited states to the ground state are shown in Fig. 2. At long distance ($R > 12$ Å), the three functions converge toward a unique value. It is about 3.44 atomic units (a.u.), corresponding to a line strength of about 23.73 a.u., in good agreement with the atomic experimental value 20.23 a.u. for $^2P_{1/2}$ atomic state.[39] The line strength of $A_{3/2}$ plus that of $B_{1/2}$ gives a value of 47.46 a.u. to be compared to 40.08 a.u., the atomic experimental of $^2P_{3/2} - ^2S_{1/2}$ transition.[39] As shown in Fig. 2, the dipole moments change slightly with the internuclear distance. The variation is about 10% for $A_{1/2} \longleftarrow X_{1/2}$ and $A_{3/2} \longleftarrow X_{1/2}$ transitions and it is about 15% for $B_{1/2} \longleftarrow X_{1/2}$ one.

Table 2. Vibrational energy levels E_v (in cm^{-1}) for the CsHe $A^2\Pi_{1/2}$ and $A^2\Pi_{3/2}$ excited molecular states. The results are compared with theoretical values from Blank *et al.*[2] and Enomoto *et al.*[38]

States	v	This work	Ref. [2]	Ref. [38]
$A^2\Pi_{1/2}$	0	47.67	50.0	48.35
$A^2\Pi_{3/2}$	0	−92.94	−95.0	−84.89
	1	−42.01	−51.1	−45.09
	2	−13.02	−25.1	−19.79
	3	−1.35	−11.06	−5.90
	4		−4.0	−0.51
	5		−0.3	

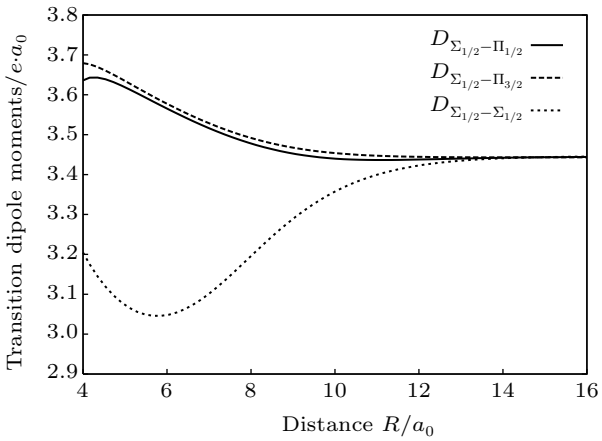

Fig. 2. Transition dipole moments $D_{\Sigma_{1/2}-\Pi_{1/2}}$, $D_{\Sigma_{1/2}-\Pi_{3/2}}$, and $D_{\Sigma_{1/2}-\Sigma_{1/2}}$ as a function of the internuclear distance R.

Table 3. CsHe equilibrium distances R_e (in Å) and potential well depths D_e (in cm^{-1}) compared with other published works.

$X^2\Sigma^+_{1/2}$		$A^2\Pi_{1/2}$				$A^2\Pi_{3/2}$		$B^2\Sigma^+_{1/2}$		Reference
R_e	D_e	R_{e1}	$^*D_{e1}$	R_{e2}	D_{e2}	R_e	D_e	R_e	D_e	
7.49	1.56	3.40	58.1	10.6	0.25	3.39	127.66	11.0	0.19	this work
6.93	9.6	3.44	51.4	9.2	1.6	3.44	125.5	10.58	0.6	[2]
7.62	1.06									[36]
		3.4				3.4				[37]
		3.49	52.2			3.49	112			[38]

* The well depth is determined from the bottom of the barrier.

4. Results and discussion

The potential-energy curves and transition dipole moments correctly built in the previous section can be utilized in the computation of the absorption and emission profiles. One has to primarily point out some important details.

4.1. Calculation details

The normalized wave functions appearing in Eqs. (1), (3), (5), and (6) are obtained by solving numerically the radial wave Eq. (4) with the Numerov algorithm,[40] and the matrix elements are computed using the Simpson rule with equally spaced intervals $\Delta R = 0.01 a_0$.

For a given temperature T, the profiles of the broadened lines at the far wings depend closely on the maximum value of the chosen rotational quantum number $J_{\max}$. Calculations show that as $J_{\max}$ increases, the intensity and the shape of the profile increase and become practically steady. The maximum rotational numbers $J_{\max} = 250$ and $J_{\max} = 25$ are enough in the calculations of the reduced absorption and emission coefficients for the free–free and free–bound transitions, respectively. In addition, one can remark that for a specific value of the rotational number J, the intensity of the profile increases when J increases and reaches its maximum for $J = 50$, then decreases gradually for J varying from $J = 50$ to $J = 250$. We note that the shape of the profile does not substantially change when J varies. We use a frequency step size $\Delta\nu = 10\,\mathrm{cm}^{-1}$ for different temperatures, and all the bound and quasibound levels are included in these calculations. In particular, the Gauss–Laguerre quadrature[41] with 100 weighted points has been used to compute the free–free integral appearing in Eqs. (1) and (5). We have also adopted the mathematical transformation used in Ref. [27] to avoid the numerical problem arising from the divergence of the matrix elements shown in the previous equations.

4.2. Classical satellite positions

At this stage, one may predict the possible existence of satellites in the far wings by adopting the classical point of view based on potential-difference curves. Indeed, satellites might appear where the curves of the potential differences between the ground and excited states exhibit extrema. Accordingly, we display in Fig. 3 the energy differences, converted into wavelengths, as a function of the internuclear distance R for vertical transitions between $A_{1/2} \longleftarrow X_{1/2}$, $A_{3/2} \longleftarrow X_{1/2}$, and $B_{1/2} \longleftarrow X_{1/2}$. This shows clearly the presence of an eventual satellite in the blue wing of the D_2 line due to the $B_{1/2} \longleftarrow X_{1/2}$ transitions. Quantitatively, a satellite should arise near the wavelength $\lambda \simeq 825$ nm from the potential variations in the short-range region close to $R \sim 7.5a_0$ in Fig. 3.

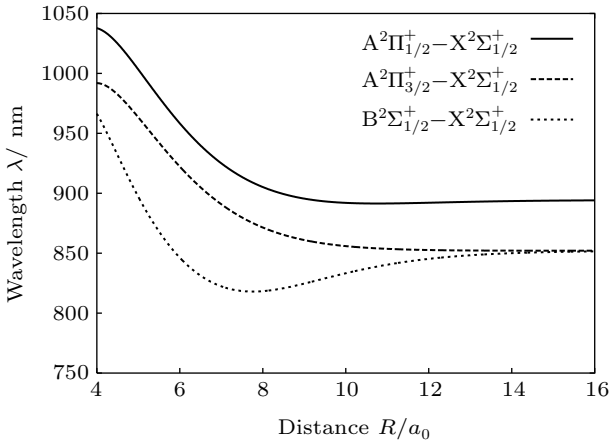

Fig. 3. Wavelengths, converted from the potential differences, for the CsHe quasi-molecular as a function of the distance R.

4.3. Absorption profiles

Generally, the photoabsorption profiles around the cesium D_1 or D_2 resonance lines are determined in the far wings by transitions from the ground to the excited CsHe molecular states, taking into account that the ground and excited molecular states are either repulsive or shallow. We may therefore consider just the transitions of the type free–free or free–bound.

More precisely, for the D_1 resonance line broadened around the wavelength $\lambda_{D_1} \simeq 894.3$ nm, the CsHe reduced absorption coefficients in the far wings are only arising from $A_{1/2} \longleftarrow X_{1/2}$. The $X_{1/2}$ electronic state is dominantly repulsive, and the $A_{1/2}$ state is slightly bound; the photoabsorption profiles are therefore resulting from the $A_{1/2} \longleftarrow X_{1/2}$ free–free and free–bound transitions. For the case of D_2 line, since the $B_{1/2}$ state is mainly repulsive and the $A_{3/2}$ state is less deep, the shapes in the far wings around the wavelength $\lambda_{D_2} \simeq 852.1$ nm are resulting from the contributions of the $A_{3/2} \longleftarrow X_{1/2}$ and $B_{1/2} \longleftarrow X_{1/2}$ free–free and the $A_{3/2} \longleftarrow X_{1/2}$ free–bound transitions.

We may mention that in both cases, and for all considered temperatures, the calculations show that the CsHe absorption spectra of the broadened D_1 and D_2 lines are largely dominated by the free–free transitions.

Nevertheless, the partial reduced absorption coefficients of the broadened D_1 line, in the range 800–1000 nm of the wavelength are presented in Fig. 4(a) for temperatures $T =$ 323 K, 448 K, 500 K, 1000 K, 2000 K, and 3000 K. It is easy to see that when we survey the graph, the profile falls quickly in the blue wing and the branches are so close together that they almost overlap, and do not depend on the temperature. In the red wing, the branches have undulated descents which disappear at low temperature, and they increase in magnitude as the temperature increases. They can be the results of the existence of the bound and, mainly, quasi-bound levels of the molecular $A_{1/2}$ state.[28]

We have illustrated in Fig. 4(b), at the same temperatures, the shape of the partial reduced absorption coefficients of the broadened D_2 line. The calculations show that the blue and red wings must result from the $B_{1/2} \longleftarrow X_{1/2}$ and $A_{3/2} \longleftarrow X_{1/2}$ free–free transitions, respectively. We are able to follow the graph from the center of the line to the wings, and we have found that the intensity of the profiles increases as the temperature increases. In particular, the spectra exhibit a satellite around the wavelength 825 nm in the blue wing for all temperatures and present undulations in the red wing. These rapid quantum oscillations are specifically due to the transitions from the potential repulsive region of $X_{1/2}$ state to the attractive $A_{3/2}$ state.

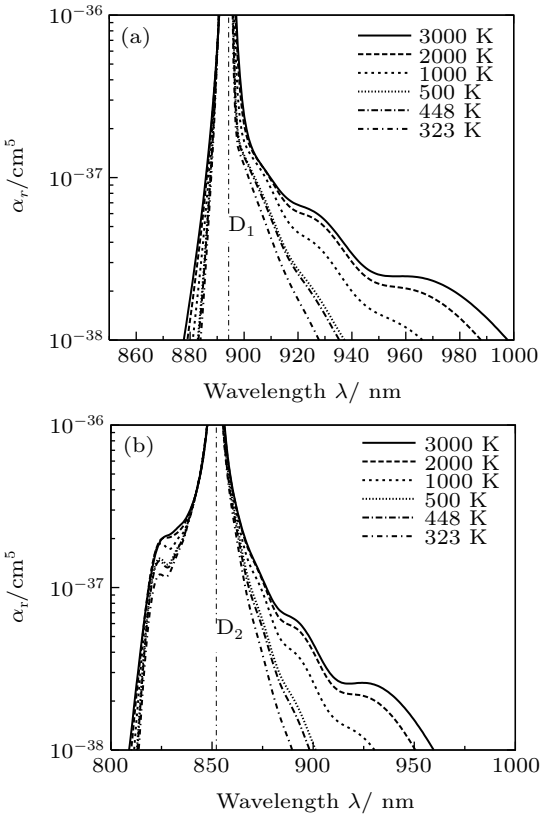

Fig. 4. Theoretical reduced photoabsorption coefficients α_r of the broadened cesium D_1 and D_2 lines in panels (a) and (b), respectively, at different temperatures.

The total absorption profile of the quasi-molecular CsHe is the sum of the partial contributions of the broadened D_1 and D_2 lines, which can be seen in Fig. 5. We notice that the total absorption spectra increase as the temperature increases and the satellite whose intensity grows with temperature begins its appearance from $T = 323$ K. Regardless of the temperature, the position of satellite does not change, which shows that the temperature has no influence on the satellite position.

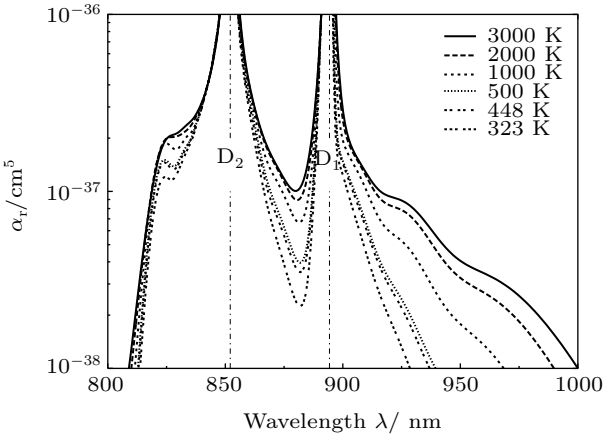

Fig. 5. Theoretical reduced photoabsorption coefficients at different temperatures.

We have at our disposal some results of previous works, as a theoretical study related to calculations of photoabsorption spectra, using a semi-classical method by Allard *et al.*[1] This study was carried out by Allard and his coworkers in the framework of the unified theory based on the potentials and dipole moments of the CsHe system calculated by Pascale.[42] They theoretically found at the temperature of 1000 K, with the low perturber density of about 10^{20} cm^{-3}, a blue-wing satellite close to the wavelength 420 cm^{-1} corresponding to 820 nm. On the other hand, Gilbert and Ch'en[43] observed experimentally a satellite in the blue wing of the CsHe profiles located around 387 ± 9 cm^{-1} which corresponds to 755 ± 18 nm. In addition, we have presented in Figs. 6(a) and 6(b) the curves of D_1 and D_2 profiles at temperature $T = 3000$ K plotted with those obtained by Allard *et al.*[1]

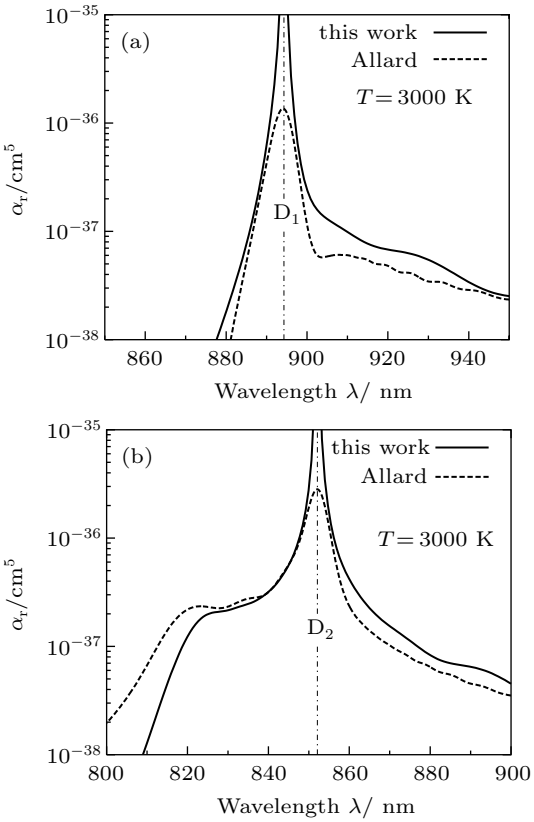

Fig. 6. Comparison of our computed $T = 3000$ K photoabsorption profiles around the cesium D_1 and D_2 lines, presented in panels (a) and (b), respectively, with those obtained within the unified theory of Allard *et al.*[1]

Moreover, Hager and his collaborator[5] have experimentally observed a satellite near the wavelength position 827 nm for Cs collisions with He at a high pressure of 2280 torr in the temperature range of 323–448 K. Figures 7(a) and 7(b) show our quantal results of D_1 and D_2 profiles at $T = 323$ K and $T = 448$ K with the experimental data points measured, in the interval of temperature $T = 323$–448 K, by Hager *et al.*[5] We can easily notice that these spectra have the same general shape and present, especially, satellite peaks in the same wings around close positions.

All these results confirm that our calculated photoabsorption spectra are in good agreement with experimental measurements and theoretical calculations, and illustrate in particular

the sensitivity of the pressure broadening calculations to the quality of potentials and the accuracy transition dipole moments we have used.

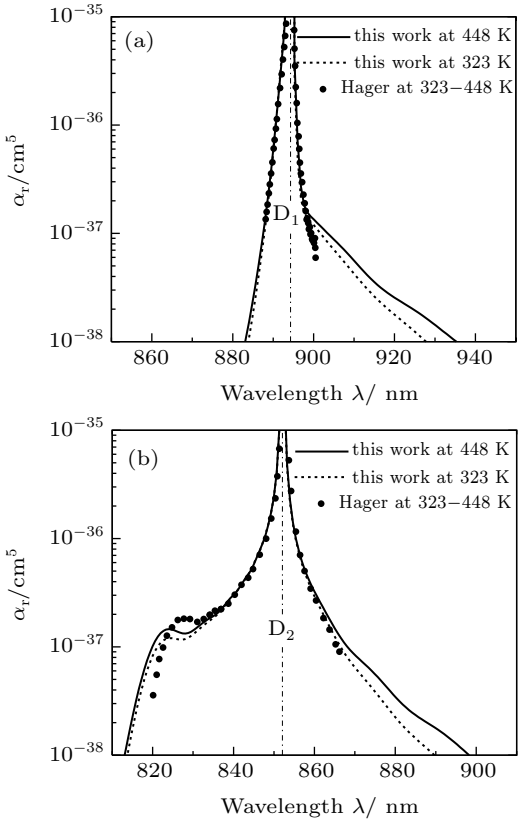

Fig. 7. Comparison of our computed photoabsorption profiles around the cesium D_1 and D_2 lines, presented in panels (a) and (b), respectively, at $T = 323$ K and $T = 448$ K, with those measured by Hager *et al.*[5]

4.4. Emission profiles

The full quantum-theoretical photoemission profiles for both broadened D_1 and D_2 resonance lines are displayed in the wavelength interval from 800 nm to 1000 nm, at temperatures $T = 323$ K, 448 K, 500 K, 1000 K, 2000 K, and 3000 K. As a matter of first importance, one needs to underline as with the CsHe absorption profile calculations that only the free–free transitions contribute to building the D_1 and D_2 emission spectra. In particular, the shapes of the emission profiles of the broadened D_1 line in the blue and red wings are constructed by $A_{1/2} \rightarrow X_{1/2}$ free–free transitions for all temperatures. As shown in Fig. 8(a), the red wing structures show undulations that virtually disappear at low temperatures, whereas in the blue wings the profiles fall quickly and become insignificant.

For the broadened D_2 resonance line, the computations state that the $A_{3/2} \rightarrow X_{1/2}$ free–free transitions are clearly dominant in the red side, while the $A_{3/2} \rightarrow X_{1/2}$ and $B_{1/2} \rightarrow X_{1/2}$ free–free transitions are significantly dominant in the blue side. Figure 8(b) displays the occurrence of satellites in the blue far wings close to the wavelength 825 nm. In addition, in the red wings, there is a shoulder whose intensity and shape vary with temperature and its position moves away from the line as the temperature increases. One may notice that the satellite positions in both emission and absorption spectra are the same. If we add up the two contributions due to the D_1 and D_2 lines, we obtain the total profile of the emission spectrum as shown in Fig. 9.

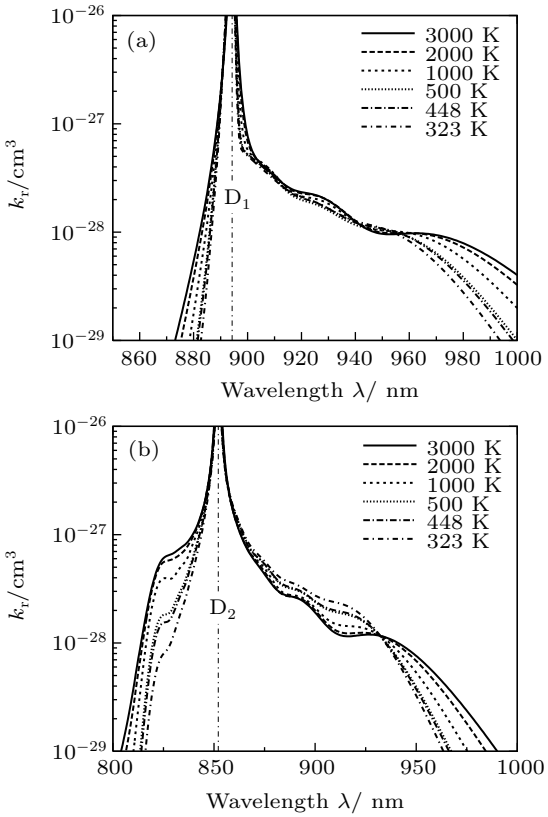

Fig. 8. Reduced photoemission coefficients k_r of theoretical reduced photoemission coefficients of the broadened rubidium D_1 and D_2 lines presented in panels (a) and (b), respectively, at different temperatures.

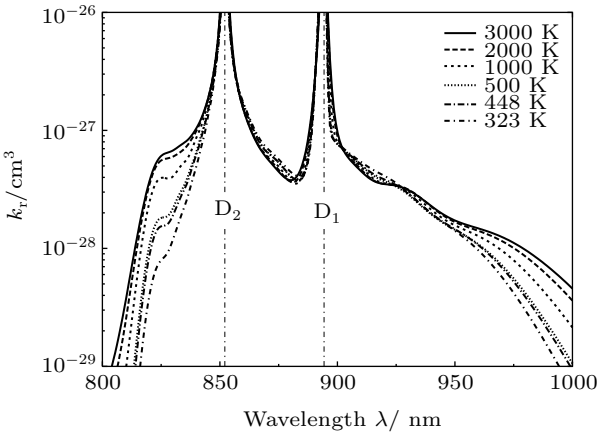

Fig. 9. Total reduced emission coefficients presented at temperatures ranging between 323 K and 3000 K.

Very recently, Blank *et al.*[2] have used the classical quasistatic approximation, based on the $B_{1/2} - X_{1/2}$ difference potential, to estimate the satellite peak position of broadened D_2 line. As a result, they calculated the blue shifted satellite

around 810.9 nm. Following a procedure described in their paper,[2] Blank and his co-workers could predict the CsHe experimental value. They foresee the value 825 nm for the CsHe experimental satellite peak.

To our knowledge, the only available experimental data of the CsHe emission profile is the normalized infinite-temperature emission spectra for 10^{19} cm^{-1} perturber density measured by Hedges *et al.*[8] To successfully reproduce the experimental spectrum at the infinite temperature ($T \to \infty$), we have estimated that the temperature of 3000 K is sufficient to be used in our calculations because the theoretically profile of the spectrum as well as its intensity does not change practically beyond this value. Finally, figures 10(a) and 10(b) show our theoretically emission profiles of D_1 and D_2 lines at 3000 K together with the experimental profiles of the same lines at infinite temperature T, respectively. It is easy to see that there is almost no difference between the D_1 and D_2 line profiles, likewise, the peaks of the two satellites in the blue wing of D_2 line are at the same locations. This shows a good agreement.

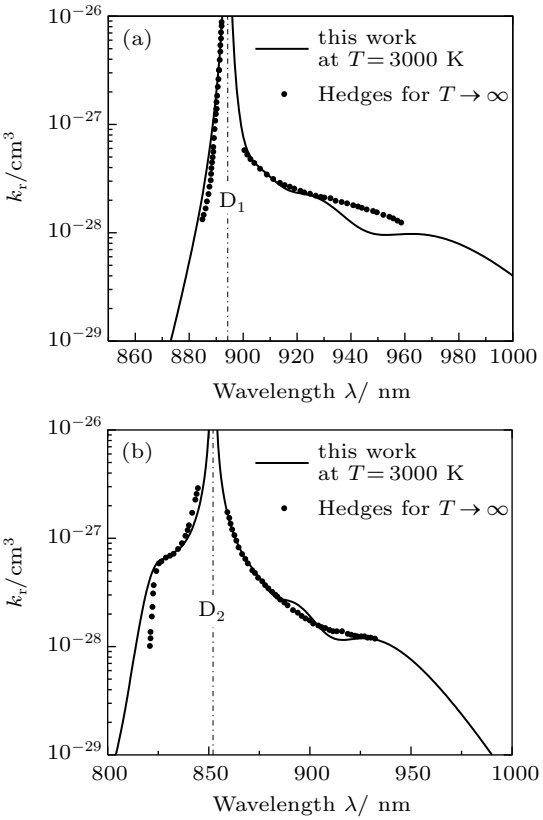

Fig. 10. Comparison of our computed $T = 3000$ K photoemission profiles around the cesium D_1 and D_2 lines, presented in panels (a) and (b), respectively, with those measured at the infinite temperature by Hedges *et al.*[8]

5. Conclusion

In this work, we have performed full quantum-mechanical calculations related to the CsHe absorption and emission profiles in the wavelength range of 800–1000 nm, at temperatures going from 323 K to 3000 K. For this purpose, we have computed accurate potential energy curves of ground $X^2\Sigma^+_{1/2}$ and excited $A^2\Pi_{1/2}$, $A^2\Pi_{3/2}$, and $B^2\Sigma^+_{1/2}$ states and the corresponding transition dipole moments using high-level *ab initio* calculations SA-CASSCF, MRCI, and SO coupling with the Davidson and the BSSE corrections. A blue satellites around 825 nm are found in the spectra of both absorption and emission which arise from the free–free $B_{1/2} \leftrightarrow X_{1/2}$ transitions. A good agreement is found with previous theoretical and experimental results.

6. Acknowledgments

This work was granted access to the HPC resources of the FLMSN, "Fédération Lyonnaise de Modélisation et Sciences Numériques", partner of EQUIPEX EQUIP@MESO, and to the "Centre de calcul CC-IN2P3" at Villeurbanne, France.

References

[1] Allard N F and Spiegelman F 2006 *Astron. Astrophys.* **452** 351
[2] Blank L and Weeks D E 2014 *Phys. Rev. A* **90** 022510
[3] Blank L, Weeks D E and Kedziora G S 2012 *J. Chem. Phys.* **136** 124315
[4] Bouhadjar F, Alioua K, Bouazza M T and Bouledroua M 2014 *J. Phys. B* **47** 185201
[5] Hager G D, Lott G E, Archibald A J, Blank L, Weeks D E and Perram G P 2014 *J. Quant. Spectrosc. Radiat. Transfer* **147** 261
[6] Zhang W, Shi Y, Hu B and Zhang Y 2018 *Chin. Phys. B* **27** 013201
[7] Miller W S, Rice C R and Perram G P 2018 *J. Quant. Spectrosc. Radiat. Transfer* **206** 151
[8] Hedges R E M, Drummond D L and Gallagher A 1972 *Phys. Rev. A* **6** 1519
[9] Rice A C, Lapp K, Rapp A, Miller W S and Perram G P 2019 *J. Quant. Spectrosc. Radiat. Transfer* **224** 550
[10] Burrows A, Burgasser A J, Kirkpatrick J D, Liebert J, Milsom A J, Sudarsky D and Hubeny I 2002 *Astrophys. J.* **573** 394
[11] Burrows A 2005 *Nature* **433** 261
[12] Allard N F, Kielkopf J F and Allard F 2007 *Eur. Phys. J. D* **44** 507
[13] Sharp C M and Burrows A 2007 *Astrophys. J. Suppl. Ser.* **168** 140
[14] Leggett S K, Saumon D, Marley M S, Lodders K, Canty J, Lucas P, Smart R L, Tinney C G, Homeier D, Allard F, Burningham B, Day-Jones A, Fegley B, Ishii M, Jones H R A, Marocco F, Pinfield D J and Tamura M 2012 *Astrophys. J.* **748** 74
[15] Allard N F, Nakayama A, Stienkemeier F, Kielkopf J F, Guillon G and Viel A 2014 *Adv. Space Res.* **54** 1290
[16] Burrows A S 2014 *Nature* **513** 345
[17] Zhdanov B V, Sell J and Knize R J 2008 *Electron. Lett.* **44** 582
[18] Zameroski N D, Hager G D, Rudolph W, Erickson C J and Hostutler D A 2011 *J. Q. S. R. T* **112** 59
[19] Zhdanov B V, Venus G, Smirnov V, Glebov L and Knize R J 2015 *Rev. Sci. Instrum.* **86** 083
[20] Yacoby E, Auslender I, Waichman K, Sadot O, Barmashenko B D and Rosenwaks SO 2018 *Opt. Express* **26** 17814
[21] Readle J D, Wagner C J, Verdeyen J T, Spinka T M, Carroll D L and Eden J G 2009 *Appl. Phys. Lett.* **94** 251112
[22] Readle J D, Verdeyen J T, Eden J G, Davis S J, Galbally-Kinney K L, Rawlins W T and Kessler W J 2009 *Opt. Lett.* **34** 3638
[23] Galbally-Kinney K L, Daniel L, Maser W J, Kessler W T and Rawlins S J D 2011 *Proc. SPIE* 7915
[24] Huang W, Tan R, Li Z and Lu X 2015 *Opt. Express* **23** 31698
[25] Werner H J, Knowles P J and Lind R 2008 *Package of ab initio Programs Molpro* version 2008.1
[26] Alioua K, Bouledroua M, Allouche A R and Aubert-Fré con M 2008 *J. Phys. B* **41** 175102
[27] Alioua K and Bouledroua M 2006 *Phys. Rev. A* **74** 032711
[28] Herman P S and Sando K M 1978 *J. Chem. Phys.* **68** 1153
[29] Sando K M 1971 *Mol. Phys.* **21** 439
[30] Woerdman J P 1985 *J. Phys. B* **18** 4205

[31] Boys S F and Bernardi F 1970 *Mol. Phys.* **19** 553
[32] Dunning Jr T H 1989 *J. Chem. Phys.* **90** 1007
[33] Lim I S, Schwerdtfeger P, Metz B and Stoll H 2005 *J. Chem. Phys.* **122** 104103
[34] Gerginov V, Calkins K, Tanner C E, McFerran J J, Diddams S, Bartels A and Hollberg L 2006 *Phys. Rev. A* **73** 032504
[35] Gerginov V, Tanner C E, Diddams S, Bartels A and Hollberg L 2005 *Opt. Lett.* **30** 1734
[36] Medvedev A A, Meshkov V V, Stolyarov A V and Heaven M C 2018 *Phys. Chem. Chem. Phys.* **20** 25974
[37] Zbiri M and Daul C 2004 *J. Chem. Phys.* **121** 11625
[38] Enomoto K, Hirano K, Kumakura M, Takahashi Y and Yabuzaki T 2002 *Phys. Rev. A* **66** 042505
[39] Rafac R J, Tanner C E, Livingston A E, Kukla K W, Berry H G and Kurtz C A 1994 *Phys. Rev. A* **50** R1976
[40] Numerov B 1932 *Bulletin of the Academy of Sciences of the USSR Science Class Mathematics and NA* **1** 1
[41] Press W H, Flannery B P, Teukolsky S A and Vetterling W T 1987 *Numerical Recipes: the Art of Scientific Computing* (New York: Cambridge University Press)
[42] Pascale J 1983 *Phys. Rev. A* **28** 632
[43] Gilbert D E and Ch'en S Y 1969 *Phys. Rev.* **188** 40